Characterization of Light-Induced, Short-Lived Interacting Radicals in the Active Site of Flavoprotein Ferredoxin-NADP + Oxidoreductase

Bo Zhuang, Daisuke Seo, Alexey Aleksandrov, Marten H. Vos

Characterization of Light-Induced Short-Lived Interacting Radicals in the Active Site of Flavoprotein Ferredoxin-NADP$^+$ Oxidoreductase

Bo Zhuang,[†] Daisuke Seo,[‡] Alexey Aleksandrov,[*,†] and Marten H. Vos[*,†]

[†]LOB, CNRS, INSERM, École Polytechnique, Institut Polytechnique de Paris, 91128 Palaiseau, France

[‡]Division of Material Science, Graduate School of Natural Science and Technology, Kanazawa University, 920-1192 Kanazawa, Ishikawa, Japan

ABSTRACT: Radicals of flavin adenine dinucleotide (FAD), as well as tyrosine and tryptophan, are widely involved as key reactive intermediates during electron transfer (ET) reactions in flavoproteins. Due to the high reactivity of these species, and their corresponding short lifetime, characterization of these intermediates in functional processes of flavoproteins is usually challenging, but can be achieved by ultrafast spectroscopic studies of light-activatable flavoproteins. In ferredoxin-NADP$^+$ oxidoreductase from *Bacillus subtilis* (*Bs*FNR), fluorescence of the FAD cofactor that very closely interacts with a neighboring tyrosine residue (Tyr50), is strongly quenched. Here we study short-lived photoproducts of this enzyme and its variants with Tyr50 replaced by tryptophan or glycine. Using time-resolved fluorescence and absorption spectroscopies, we show that upon the excitation of WT *Bs*FNR, ultrafast ET from Tyr50 to the excited FAD cofactor occurs in ~260 fs, an order of magnitude faster than the decay by charge recombination, facilitating the characterization of the reaction intermediates in the charge-separated state with respect to other recently studied systems. These studies are corroborated by experiments on the Y50W mutant protein, which yield photoproducts qualitatively similar to those observed in other tryptophan bearing flavoproteins. By combining the experimental results with molecular dynamics simulations and quantum mechanics calculations, we investigate in detail the effect of protein environment and relaxations on the spectral properties of those radical intermediates, and demonstrate that the spectral features of radical anionic FAD are highly sensitive to its environment, and in particular to the dynamics and nature of the counter-ions formed in the photoproducts. Altogether, comprehensive characterizations are provided for important radical intermediates that are generally involved in functional processes of flavoproteins.

INTRODUCTION

Electron transfer (ET) reactions in proteins are pivotal steps in a wide array of biochemical processes, including for instance photosynthesis and aerobic respiration.[1] These reactions always involve specialized cofactors as redox centers, but can also employ amino acid radicals as intermediates.[2–6] In general, the latter are short-lived in nature and therefore difficult to characterize during biochemical reactions that are limited by reactant binding dynamics. However, in light-induced reaction chains, short-lived intermediates may be more readily accumulated using short light pulses. For instance, in proteins bearing flavin as a cofactor, flavin photoreduction by ET from nearby tyrosine (TyrOH) or tryptophan (TrpH) to excited flavin is an efficient fluorescence quenching pathway.[7–13] Such pathways are operational in several light-sensitive biological functions, as demonstrated by studies of DNA photolyase,[14,15] cryptochrome[12] and BLUF domain proteins.[17,18] Yet, flavin photoreduction can also occur in the vast majority of flavoproteins that are not functionally light-active. In those proteins, the flavin photochemical properties can also be exploited, for instance as a tool to explore the conformational dynamics of the active site, as ET reactions are highly sensitive to the relative positions and conformations of donors and acceptors.[19,20] A schematic representation of possible light-induced reactions involving flavin and redox-active amino acids is given in Figure 1.

The involvement of the aromatic residues tyrosine and tryptophan in these light-induced processes also make them suitable model systems to investigate the properties of tyrosyl or tryptophanyl radical intermediates and their interactions with corresponding flavin radicals when they coexist as radical pairs. It has been shown that upon the excitation of semi-reduced CPD photolyase, the photoreduction reaction proceeds by successive ET steps along a chain of three conserved tryptophan residues, whereby both the protonated ($TrpH^{\bullet+}$) and the deprotonated ($Trp^{\bullet}$) tryptophanyl radicals (pKa ~4) can be generated sequentially on the picosecond-nanosecond timescale;[14] in some cases, deprotonated tyrosyl radicals can be observed in such proteins as well.[21] Similar reaction products have later also been observed upon excitation of oxidized flavin in the related cryptochrome blue-light sensors.[16,22,23] More recently, the flavin excited state quenching by tryptophan has been examined in detail in artificial protein maquettes.[24,25] In contrast to tryptophan, for a long time it had been assumed that the oxidation of tyrosine is necessarily accompanied by a concerted deprotonation due to its extremely low pKa (~−2). However, recent full spectral studies of modified bacterial tRNA methyltransferase, TrmFO[26,27], have spectroscopically identified a transiently formed protonated tyrosyl radical ($TyrOH^{\bullet+}$). Subsequently, this form was also assigned to transient features in the popular model flavoprotein glucose oxidase.[28] Nevertheless, in the latter reports, the formation and decay rates of the initial product state are very close, complicating the spectral disentanglement of this state, and also did not compare tyrosine and tryptophan in the same protein site. The present study was undertaken on a flavoprotein

that has not been investigated by ultrafast spectroscopies before, but harbors extremely close-lying redox partners involved in quenching, allowing better kinetic separation. We further investigate the influence of this proximity on the spectral properties of flavin, tyrosine and tryptophan radical intermediates.

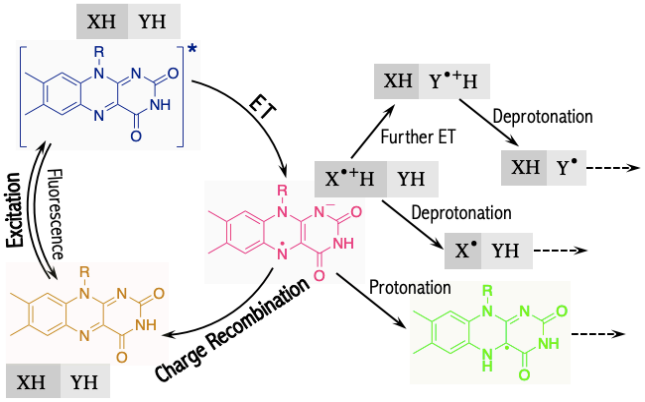

Figure 1. General reaction pathways for light-induced processes in flavoproteins. Flavin is represented by the isoalloxazine moiety. XH and YH stand for aromatic residues (tryptophan or tyrosine), for simplicity limited to two. Anion protonation and cation deprotonation may be coupled, corresponding to proton transfer from residue to flavin (not explicitly depicted). For simplicity back reactions beyond the primary radical pair are not shown.

Ferredoxin-NADP$^+$ oxidoreductase from *Bacillus subtilis* (*Bs*FNR) is a homo-dimeric flavoprotein homologous to bacterial NADPH-thioredoxin reductase.[29] It catalyzes the redox reaction between the electron carrier nucleotide NADP$^+$/H and ferredoxin, a small iron-sulfur protein that also mediates ET.[30,31] A high-resolution structure of wild-type (WT) *Bs*FNR is available.[32] A functionally relevant tyrosine residue (Tyr50) is found to locate extremely close (shortest distance between ring atoms: 3.3 Å) to the flavin adenine dinucleotide (FAD) cofactor, forming an unusual π–π stacking interaction with the isoalloxazine ring. Whereas the protein does not form known functional photoproducts, Tyr50 has been shown to strongly quench FAD fluorescence. Variants where this residue is replaced by tryptophan and glycine are also available and tryptophan can act as a quencher as well.[33] These properties make *Bs*FNR a suitable model system to characterize the short-lived intermediates during the light-induced processes using ultrafast spectroscopy. Here we present for the first time a full spectral investigation of light-induced dynamics in WT *Bs*FNR, and its Y50W and Y50G variants. We show that the initial photoreduction occurs predominantly on a timescale of ~200 fs, much faster than charge recombination occurring in a few picoseconds, thus allowing straightforward spectroscopic characterization of the initial photoproducts involving radical anionic FAD (FAD$^{\bullet-}$), TyrOH$^{\bullet+}$ and TrpH$^{\bullet+}$.

Moreover, although the ET kinetics in flavin binding proteins have been investigated in depth by adopting classical and quantum chemistry simulation approaches,[8,13,34] the spectral properties of the reaction intermediates remain largely unaddressed from a theoretical standpoint. Herein, by combining Molecular Dynamics (MD) simulations and a hybrid Quantum Mechanics/Molecular Mechanics (QM/MM) approach, our experimental findings are further explored to obtain detailed insights into the properties of interacting radical intermediates in a protein environment.

EXPERIMENTAL METHODS

Sample Preparations. WT *Bs*FNR and Y50W and Y50G mutant proteins were prepared as described previously.[33] All spectroscopic measurements were performed under air atmosphere in a quartz cell of 1 mm path length, at room temperature. The optical density of the samples was adjusted to ~0.2 at 390 nm for the transient fluorescence and transient absorption experiments.

Spectroscopic Measurements. Steady-state absorption spectra were taken using a Shimadzu UV-vis 1700 spectrometer.

The setup for time-resolved fluorescence employing a Kerr gate was described previously.[35] Briefly, part of the 780 nm output from the Ti:sapphire laser/amplifier system (Quantronix Integra-C) operating at 0.5 kHz was passed through a BBO crystal, yielding an excitation pulse centered at 390 nm. The remaining 780 nm beam was directed through a motorized delay-line and focused into the Kerr medium where it spatially overlapped the fluorescence from the sample. Kerr media with different time-resolution/sensitivity compromises were used, *i.e.*, suprasil (response time ~200 fs) and CS_2 (response time ~1 ps).

Multicolor time-resolved absorption spectra were recorded by the pump-probe technique on an instrument operating at 500 Hz, as described previously.[27] Similar to the time-resolved fluorescence experiment the pump pulses were centered at 390 nm. Continuum broadband pulses were used as the probe. Pump and probe beams were set at the magic angle (54.7°) to record the isotropic spectra. The excitation power was adapted such that each shot of the pump beam excited less than 10% of the sample. The concentrations of excited molecules were determined using $[Ru(bpy)_3]Cl_2$ as a reference.[26,36] Global analysis of the data from time-resolved spectroscopic measurements was performed using the Glotaran program based on the R-package TIMP.[37]

Computer Simulations. The structure of WT *Bs*FNR was taken from the Protein Data Bank (PDB entry: 3LZW; resolution: 1.8 Å). MD simulations were carried out for WT *Bs*FNR and the Y50W mutant using the NAMD programs (version 2.13).[38] Protein residues within a 24 Å sphere centered at the isoalloxazine ring of FAD were placed in an 80 Å cubic box of water. Non-hydrogen atoms between 20 and 24 Å from the sphere center were harmonically restrained to their experimentally determined positions based on the crystal structure. Periodic boundary conditions were assumed, and an appropriate amount of potassium counter-ions were included to render the system electrically neutral. The CHARMM36 force field[39] was used for the protein residues and the TIP3P model for water;[40] a recently developed force field for flavins was used to describe FAD.[41] The starting structure of Y50W *Bs*FNR was built using the structure of WT *Bs*FNR by replacing the Tyr50 residue by tryptophan. Different orientations of Trp50 were generated using the SCWRL4 program,[42] adjusted to be parallel to that of the original tyrosine, and further subjected to MD simulations (see Section 1 of Supporting Information for details). All the MD simulations were performed at a constant temperature of 295 K and pressure of 1 atm. after 500 ps of thermalization and with time step of 2 fs.

To simulate the relaxation processes after ET, force field parameters in the model were switched to correspond to the charge-separated state. For FAD$^{\bullet-}$ relevant parameters are included in the aforementioned flavin force field; for TyrOH$^{\bullet+}$ and TrpH$^{\bullet+}$, CHELPG atomic charges[43] were obtained after QM

level geometry optimization in vacuum (see Section 6 of Supporting information for details). Subsequently the model was relaxed with 10 ps MD simulations starting from the neutral state geometry. QM/MM calculations were performed with the pDynamo program (version 1.9.0)[44] coupled with the ORCA package (version 4.0.1.2).[45] QM-MM electrostatic interaction were treated using the electrostatic embedding. The QM region included the isoalloxazine ring moiety of FAD or the side chain of the target residue (Tyr50 and Trp50 in WT *Bs*FNR and the Y50W mutant, respectively) in the radical anionic or radical cationic states, respectively. Excitation energies and oscillator strengths of 30 excited states were then estimated using time-dependent density functional theory (TDDFT) with the unrestricted hybrid exchange-correlation functional B3LYP.[46] Unless stated otherwise, the 6-31+G* basis set was used for the radical anions and 6-311G* for the radical cations.[47] The remaining protein components and water molecules (201 residues and ~14210 water molecules) were included into the MM region and described with the same force fields as in the MD simulations. Protein structures from 100 equally spaced snapshots along the stabilized MD trajectories of 100 ns were used as input for the QM/MM calculations; excitation energies and oscillator strengths calculated for those snapshots were broadened with a Gaussian line shape (FWHM: 0.35 eV for radical anions and 0.50 eV for radical cations, corresponding to the width of the experimental spectra) and then averaged. The same MD and QM/MM protocols were also applied to a dipeptide with a tryptophan side chain, to simulate the $TrpH^{\bullet+}$ absorption spectra in a solvent environment using the explicit solvent model. We also tested the effect of geometry optimization on computed spectra by comparing the results with and without energy minimization at the QM level of theory as described in Section 7 of Supporting Information. Additionally, the ORCA package was used to evaluate the effect of a nearby point charge on the absorption spectra of $FAD^{\bullet-}$, $TyrOH^{\bullet+}$ and $TrpH^{\bullet+}$ in vacuum and in the implicit solvent. For these calculations, analogues containing the functional chromophore groups of FAD, tyrosine and tryptophan were used as simplified models. TDDFT calculations were carried out at UB3LYP/6-31+G* level after structural optimizations at the same level in vacuum or with the CPCM implicit solvent model[48] where a dielectric constant ε=20 was used to simulate the screening effect of the protein/solvent environment.

RESULTS

Structural Dynamics of WT and Y50W *Bs*FNR. In the crystal structure of WT *Bs*FNR, Tyr50 stacks almost in parallel on the *si*-face of the isoalloxazine ring moiety of FAD, assisted by a hydrogen bond interaction between its OH group and the O2´ hydroxyl group of the ribityl moiety of FAD (Figure 2a). Previous studies have found that Tyr50 plays an important role in the functioning of the protein by stabilizing the FAD cofactor in different redox states.[33] Throughout the 120 ns MD simulation of WT *Bs*FNR, the stacking conformation of Tyr50 with the isoalloxazine ring moiety of FAD was well-preserved, with a variation in minimal ring-to-ring distances limited to a range between 3.0 and 3.8 Å (Figure 3). The average distance of 3.4 Å in MD simulations between FAD and Tyr50 rings compares well with the distance in the crystal structure of 3.3 Å. Here the minimal ring-to-ring distance is defined as the shortest distance between any non-hydrogen atoms from two rings, which is thought to be relevant to the electronic coupling determining the electron transfer rate. Other aromatic residues that could potentially act as the electron donors, *e.g.*, Tyr25, Tyr56, and Trp169, are highly unlikely to compete with Tyr50 during the photoreduction of FAD on the sub-picosecond timescale due to much longer donor-acceptor distances and unfavorable conformations.

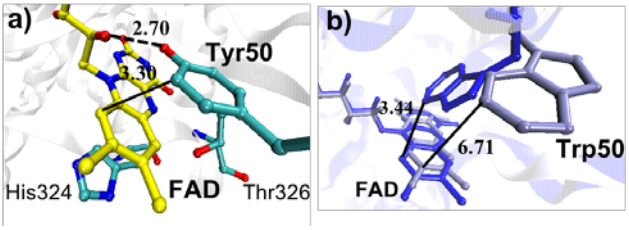

Figure 2. (a) The active site of WT *Bs*FNR in the crystal structure (PDB entry: 3LZW). (b) Superimposed structures with two conformations in the active site of Y50W *Bs*FNR from MD simulations. The important distances are shown in Å.

Because no crystal structure of the Y50W mutant is available, it was modeled by replacing Tyr50 in the crystal structure of WT *Bs*FNR by a tryptophan (Trp50). As described in Section 1 of Supporting Information, there are two possible orientations of the tryptophan plane parallel to that of the original tyrosine (Figure S5a), which were examined by MD simulations. Notably, during simulations of one of the models Trp50 rotated after a short equilibration MD (~0.5 ns), as shown in Figure S5b, and further exhibited structural dynamics similar to that of the other initial model. Thus, the two initial models converged to a very similar structure; this model was exploited for further analysis.

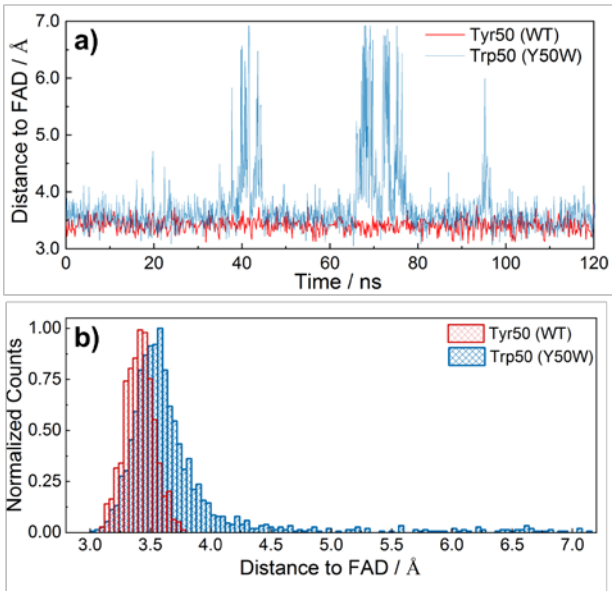

Figure 3. The minimal ring-to-ring distance (a) and distribution (b) between FAD and Tyr50 and Trp50 in MD simulations of WT and Y50W *Bs*FNR respectively.

In our simulations, the ring-to-ring distance between Trp50 and FAD demonstrates large fluctuations on the multi-nanosecond timescale with a distribution extending to much further than that between Tyr50 and FAD in WT *Bs*FNR (Figure 3), indicating that in the Y50W mutant the tryptophan is not well stabilized in the position corresponding to Tyr50. This can be rationalized by the absence of proper hydrogen bond and stacking interactions between FAD and the tryptophan. Although most of

the time (~90%) throughout the simulation Trp50 and FAD remain at less than 4 Å away, there were short periods where Trp50 moved outwards and located relatively distant from FAD (> 5 Å; Figure 2b, blue *versus* purple). Additionally, substantial structural fluctuations of the FAD cofactor during the MD simulation of the Y50W mutant protein were observed as well (Figure S5c), which is in agreement with the fact that the presence of Tyr50 stabilizes the isoalloxazine ring by stacking interactions.[33,49]

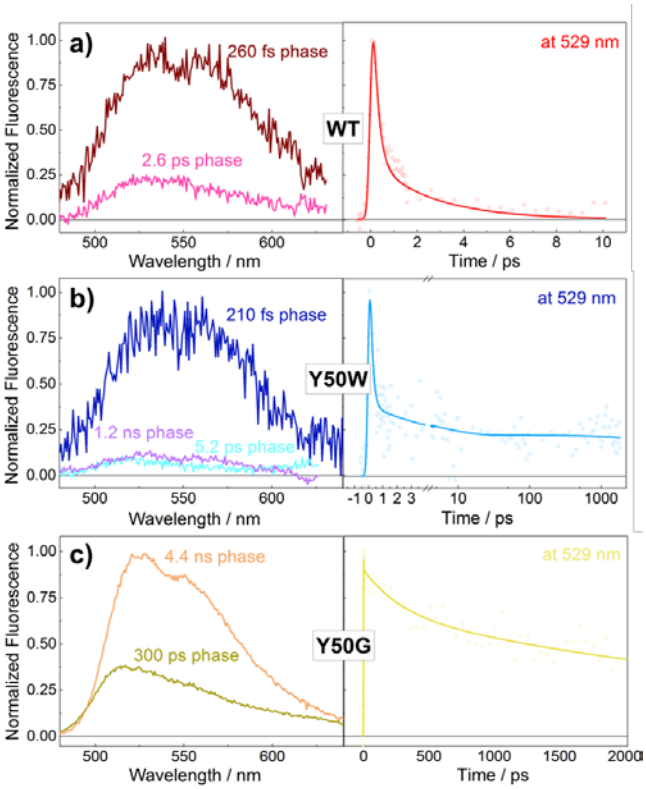

Figure 4. Decay associated spectra (DAS) from the global analysis of fluorescence decays (Left) and kinetic traces at 529 nm (Right) of WT (a), Y50W (b, linear-logarithmic timescale) and Y50G (c) *Bs*FNR.

Time-Resolved Fluorescence. As reported in previous work, the steady-state fluorescence intensity of the protein-bound FAD in Y50G *Bs*FNR is six to seven times as high as that of free FAD, while in WT and Y50W *Bs*FNR mutant fluorescence intensities decrease to <3% and 9%, respectively, of that of free FAD.[33] These observations are fully consistent with the results of time-resolved fluorescence in our study (Figure 4 and Table 1). The fluorescence decay of excited FAD (FAD^*) in WT and Y50W *Bs*FNR is dominated (>80%) by very fast phases, fitted with time constants of 260 fs and 210 fs respectively. For WT a minor phase with a time constant of 2.6 ps is also observed. In Y50W *Bs*FNR, the fluorescence decay is more multiphasic, with additional time constants of 5.2 ps, and 1.2 ns. On the other hand, in Y50G *Bs*FNR where a close-lying redox-active aromatic residue is absent, an overall much slower bi-exponential decay was detected, with time constants of 300 ps and 4.4 ns (dominant phase). These findings clearly show that Tyr50 and Trp50 in WT *Bs*FNR and the Y50W mutant are the main electron donors to FAD^* and lead to efficient fluorescence quenching. The observed multiphasic fluorescence decay with a long-lived component in Y50W *Bs*FNR is generally consistent with our MD simulations, where we observed substantial conformational heterogeneity of the Trp50-FAD pair. As is the general case in flavoenzymes, the coexistence of multiple configurations of flavin-electron donor pairs results in a multiphasic fluorescence decay.[19,20] In particular, in those Y50W *Bs*FNR proteins where the Trp50 is distant from FAD, the fluorescence quenching is expected to be much less efficient.

Furthermore, in the case of Y50G *Bs*FNR, the 300 ps phase that accounts for ~30% of the fluorescence decay is still faster than expected for nonquenched unstacked FAD (a few nanoseconds, as observed in the dominant longer phase), suggesting the existence of less efficient yet active electron donors located further away (candidates include Tyr25 and Tyr56).

Effect of Product Binding. The addition of the reaction product $NADP^+$ to *Bs*FNR induces changes in the transition bands of FAD in proteins, indicating the binding of $NADP^+$ to the active site.[33] The influence of $NADP^+$ binding on the active-site conformations was also examined using time-resolved fluorescence spectroscopy. As summarized in Table 1 and Figure S6, the fluorescence decays with and without $NADP^+$ are nearly identical in WT *Bs*FNR; hence the presence of $NADP^+$ does not significantly alter the interaction between FAD and Tyr50. However, in the Y50W and Y50G mutants, the fluorescence decays in a different manner when $NADP^+$ is present. After the $NADP^+$ binding, the fluorescence decay of Y50W *Bs*FNR remained multiphasic but became noisier and the long-lived component strongly increased, probably due to increased conformational heterogeneity and/or FAD dissociation. Together these results indicate that in this system the binding of $NADP^+$ is likely to displace Trp50 and significantly alter the active-site conformation. This finding also corroborates the result of the MD simulations that Trp50 positions differently in the protein than Tyr50.

Table 1. Parameters from the global multi-exponential fit of time-resolved fluorescence decays in WT *Bs*FNR and its Y50W and Y50G mutants

	τ_1 (ps)[a]	τ_2 (ps)[a]	τ_3 (ps)[a]
WT	0.26 (0.86)	2.60 (0.14)	
WT + $NADP^+$	0.23 (0.88)	2.60 (0.12)	
Y50W	0.21 (0.80)	5.2 (0.09)	1200 (0.11)
Y50W + $NADP^+$	0.35 (0.64)	2500 (0.36)	
Y50G	300 (0.26)	4400 (0.74)	
Y50G + $NADP^+$	2500 (1.00)		

[a]The pre-exponential factor of each component is given in parentheses.

Upon $NADP^+$ addition, the fluorescence decay of Y50G *Bs*FNR, on the other hand, changed from biphasic to monophasic, notably abolishing the faster 300 ps phase. A possible interpretation is that in Y50G *Bs*FNR, the $NADP^+$ binding is not compatible with the configuration where FAD^* can be quenched by a remote electron donor (as mentioned above), and hence $NADP^+$ binding impedes structural heterogeneity.

In the crystal structure of WT *Bs*FNR in complex with $NADP^+$ (PDB entry: 3LZW), the $NADP^+$ product is located far (> 10 Å) away from the isoalloxazine ring of FAD. Yet, there is considerable discussion in the field whether this structure represents the dominant binding conformation in solution or whether hydride transfer would occur through short-lived flavin-substrate contacts.[50,51] We performed 50 ns MD simulations

based on the NADP$^+$-complexed crystal structure of WT *Bs*FNR and found that at the remote binding position NADP$^+$ has no noticeable effect on the configuration of FAD and Tyr50 in WT *Bs*FNR (Figure S4). We foresee more extensive investigations of the dynamics of NADP$^+$-flavin interactions.

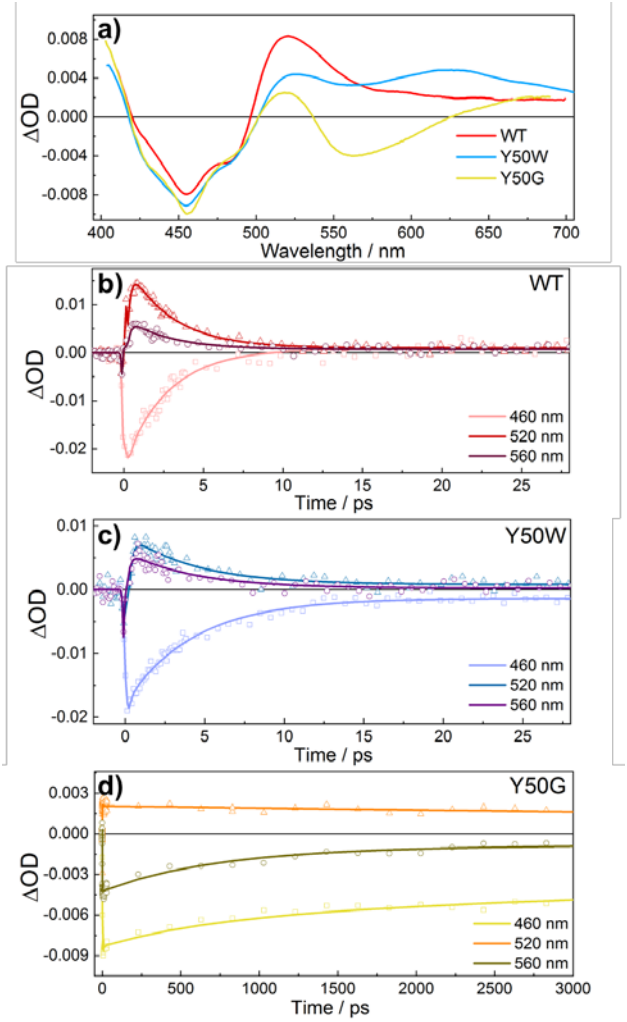

Figure 5. Isotropic transient absorption spectra of *Bs*FNR variants measured at 3 ps after excitation (a), and kinetic traces of WT (b), Y50W (c) and Y50G (d) *Bs*FNR at selected wavelengths.

Transient Absorption Spectroscopy. As fluorescence decays only provide information on excited state kinetics, to characterize the transient species during the light-induced process of *Bs*FNR, we performed transient absorption spectroscopic measurements. Figure 5 shows the isotropic transient absorption spectra of *Bs*FNR in WT, Y50W and Y50G variants recorded 3 ps after excitation, as well as kinetic traces at selected wavelengths. In the transient spectra, the negative bands around 450 nm are dominated by ground state bleaching (GSB). The spectrum of Y50G *Bs*FNR contains an additional negative band around 560 nm that is assigned to the stimulated emission (SE), as well as induced absorption features below 420 nm, around 525 nm and beyond 625 nm that are assigned to the absorption of FAD*. The shape of these features remains fairly unchanged up to the nanosecond timescale (Figure S7), indicating the persistence of a long-lived FAD* population, in agreement with the time-resolved fluorescence experiments (Figure 4). On the nanosecond timescale the absorption in the red spectral range increases, which we assign to formation of some triplet state after intersystem crossing.

In contrast to Y50G *Bs*FNR, in the 3 ps spectra of WT and Y50W *Bs*FNR the SE signal does not clearly appear, whereas distinct positive signals beyond 500 nm are observed. This indicates that in these systems the dominant FAD* decay on the femtosecond timescale leads to new photoproducts, which can be attributed to ET from different nearby electron donors.

Multi-exponential global analysis of these transient absorption data was performed. The resulting evolution associated spectra (EAS, reflecting the difference spectra of the precursor of the exponential phase and the initial state assuming a linear reaction scheme) of the product states are given in Figure 6 and Figure S7. Reference spectra of intermediate species that are generally involved in the photochemistry of flavoproteins are summarized in Figure 7.

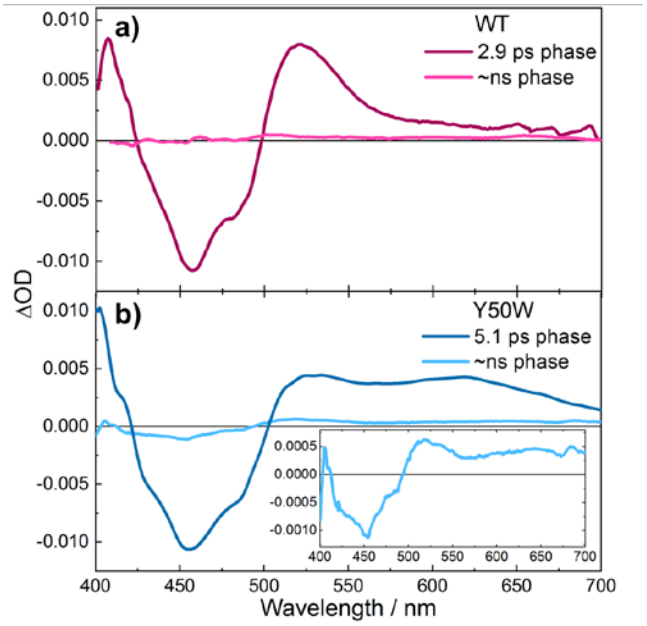

Figure 6. EAS of the picosecond and long-lived phases obtained from global analysis of transient absorption data of WT (a) and Y50W (b) *Bs*FNR; inset panel: magnified long-lived phase.

The transient absorption data of WT *Bs*FNR were fitted by two kinetic phases, with time constants of 240 fs and 2.9 ps, and a long-lived phase. The 240 fs phase, required to obtain a satisfactory fit, has a similar time constant as the dominant fluorescence decay phase (260 fs) and can be assigned to FAD* decay. The time constant is close to the instrument response function, therefore the corresponding EAS (Figure S7) shows strong modulations due to cross-phase modulation artefacts during pump-probe temporal overlap. As mentioned above, the 2.9 ps phase EAS (Figure 6a) predominately reflects decay of a product state, with only a modest contribution expected from the excited state (~14%, estimated from fluorescence decays). As Tyr50 is the electron donor responsible for quenching FAD*, the product state should be the FAD$^{\bullet-}$/TyrOH$^{\bullet+}$ ion pair or derivatives thereof. TyrOH$^{\bullet+}$ may in principle become deprotonated concertedly with its formation to yield TyrO$^\bullet$. The only nearby candidate proton acceptor is the flavin with which Tyr50 closely interacts; it is H-bonded to the O2´ hydroxyl group of the ribityl moiety of FAD. Yet, the EAS does not show the characteristic absorption band of FADH$^\bullet$ between 600 and 700 nm.

We infer that the photoproducts in the 2.9 ps phase EAS are $FAD^{\bullet-}$ and the tyrosyl cation radical $TyrOH^{\bullet+}$. We note that the induced absorption band centered at ~520 nm that may include contributions from both species, extends more to the longer wavelengths than the spectral features of $FAD^{\bullet-}$ in glucose oxidase (GOX) and in insect cryptochrome (CRY) in Figure 7. It is also qualitatively similar, but more red-extended in the induced absorption part, to the transient spectrum assigned to the $FAD^{\bullet-}/TyrOH^{\bullet+}$ ion pair in a TrmFO variant.[27] This issue will be addressed below. Finally, the remaining long-lived phase is too small (<1% of the initial signal in the bleaching area) to be reliably analyzed.

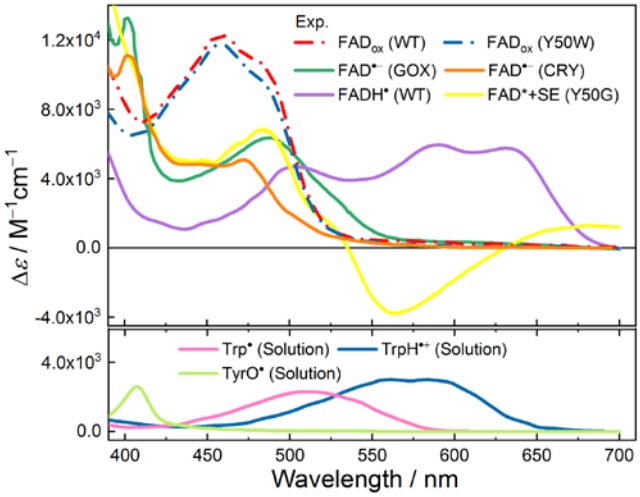

Figure 7. Reference absorption spectra of flavin (top) and aromatic amino acid (bottom) intermediate species usually involved in the light-induced processes in flavoproteins. Steady-state spectra of $FAD^{\bullet-}$ in glucose oxidase (GOX)[52] and insect cryptochrome (CRY),[53] $TyrO^{\bullet}$, $Trp^{\bullet}$, $TrpH^{\bullet+}$ in solution,[54–56] as well as $FADH^{\bullet}$ in WT *Bs*FNR,[31] are taken or derived from published data. The spectrum of FAD^{*} absorption and the corresponding SE band are extracted from the transient absorption spectrum of Y50G *Bs*FNR (see Section 4 of Supporting Information). The $S_0 \rightarrow S_1$ transition bands of ground-state FAD (FAD_{ox}) in WT *Bs*FNR and the Y50W mutant are also shown for comparison (full spectra provided in Figure S1).

For Y50W *Bs*FNR, two kinetic phases with time constants of 200 fs, 5.1 ps, and a long-lived phase are required to fit the transient absorption data. The 200 fs phase, similar to WT *Bs*FNR, represents the dominant initial excited state decay due to ultrafast ET, consistent with the fluorescence decay. Similar to the 2.9 ps phase of WT *Bs*FNR, the 5.1 ps phase in the Y50W mutant is clearly dominated by product state contributions. The broad induced absorption in the red part of the spectrum (Figure 6b) is in general agreement with $TrpH^{\bullet+}$ formation, but also may reflect $FADH^{\bullet}$ formation (Figure 7). Thus, at first view, both ET (with product state of $FAD^{\bullet-}/TrpH^{\bullet+}$ ion pair) and concerted proton-electron transfer (CPET, with product state $FADH^{\bullet}/Trp^{\bullet}$ radical pair) are possible. Yet, given the higher p*K*a of $TrpH^{\bullet+}$ than $TyrOH^{\bullet+}$ and the modeled more distant interaction of Trp50 than Tyr50 with the flavin ring (Figure 3), CPET appears (even) less likely to occur on the sub-picosecond timescale than $FADH^{\bullet}/TyrO^{\bullet}$ formation in WT *Bs*FNR.

We further investigated this issue by a detailed spectral analysis (Figure 8). By assuming an ET reaction and taking into account partial contributions from FAD^{*} absorption and SE, the 5.1 phase EAS can be represented according to Equation (1).

$$EAS_{5.1ps}^{(ET,Y50W)} = [\Phi_1(\varepsilon_{FAD^{\bullet-}} + \varepsilon_{TrpH^{\bullet+}}) + \Phi_2\Delta\varepsilon_{FAD^{*}/SE} - (\Phi_1+\Phi_2)\varepsilon_{FAD_{ox}^{Y50W}}]c_0L \quad (1)$$

Likewise, by assuming a CPET reaction, the EAS can be represented as:

$$EAS_{5.1ps}^{(CPET,Y50W)} = [\Phi_1(\varepsilon_{FADH^{\bullet}} + \varepsilon_{Trp^{\bullet}}) + \Phi_2\Delta\varepsilon_{FAD^{*}/SE} - (\Phi_1+\Phi_2)\varepsilon_{FAD_{ox}^{Y50W}}]c_0L \quad (2)$$

where c_0 is the initial concentration of FAD^{*} after the excitation at 390 nm, ε_i are the molar extinction coefficient of species *i*, Φ_1 is the quantum yield of the initial ET or CPET reaction, Φ_2 is the molar ratio of FAD^{*} that decays with a lifetime similar to the charge recombination (*vide supra*), *L* is the optical path, and $\Delta\varepsilon_{FAD^{*}/SE}$ gives the differential molar extinction coefficient with both the contributions from the FAD^{*} and SE. Here, as described in Section 4 of Supporting Information, c_0 is determined using an actinometric reference $[Ru(bpy)_3]Cl_2$, and Φ_1, Φ_2 are inferred from the time-resolved fluorescence analysis (Table 1) to be 0.80 and 0.09, respectively. The $\Delta\varepsilon_{FAD^{*}/SE}$ is extracted from the transient absorption spectrum of Y50G *Bs*FNR, published results of molar extinction coefficients of $TrpH^{\bullet+}$ and $Trp^{\bullet}$ in solution, as well as $FAD^{\bullet-}$ in GOX were used to represent corresponding species (Figure 7). With all parameters and spectra on the right-hand side of the equations determined, we are able to construct quantitative model spectra.

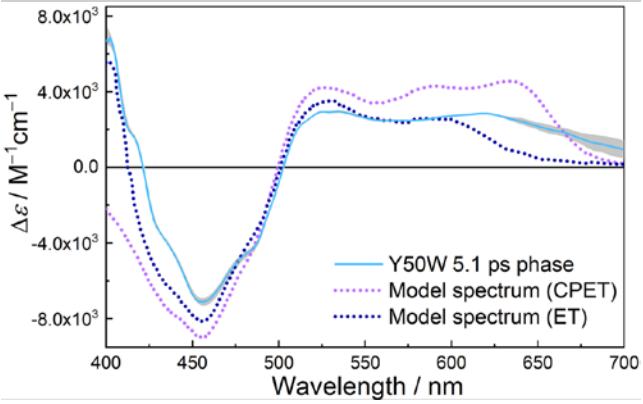

Figure 8. Spectral analysis of the 5.1 ps phase EAS of Y50W *Bs*FNR. Model spectra with ET and CPET pathways were constructed according to Equation (1) and (2). The estimated confidence interval is shaded in grey.

As illustrated in Figure 8, modeling the 5.1 ps phase EAS with contributions from $Trp^{\bullet}$ and $FADH^{\bullet}$ cannot explain the strong positive absorption around 410 nm, and the experimental feature around 625 nm does not match that in the model. In contrast, assuming that only ET occurs in this ultrafast timescale, the model spectrum with photoproducts of $TrpH^{\bullet+}$ and $FAD^{\bullet-}$ reproduces the GSB, and induced absorptions at around 410 nm and up to 600 nm in the EAS, rather satisfactorily. However, a bathochromic shift (red-shift) or spectral broadening to longer wavelength is required to account for the absorption band that extend beyond 650 nm. As indicated in the Discussion section below, such shifts in the $TrpH^{\bullet+}$ absorption spectrum have been invoked before in other systems. Altogether, the photoproducts that appear in the 5.1 phase can be reasonably assigned to recombination of a $FAD^{\bullet-}/TrpH^{\bullet+}$ ion pair. The origin of the $TrpH^{\bullet+}$ shift will be further addressed below.

Finally, a small but significant long-lived phase is observed. This phase likely contains contributions from the fraction of the

protein with long-live fluorescence, where Trp50 lies relatively far away from FAD and cannot donate electrons efficiently. The EAS of this phase (see the inset of Figure 6b) indeed shows a more pronounced SE feature between 550 and 600 nm compared to that of 5.1 ps phase. Furthermore, more long-lived product states clearly also contribute to this phase. No attempt was made to further model this small phase.

Scheme 1. Proposed reaction scheme of light-induced process of WT *Bs*FNR (red) and the Y50W variant (blue, in parentheses). For multiphasic ET, only the lifetimes of the main components are shown.

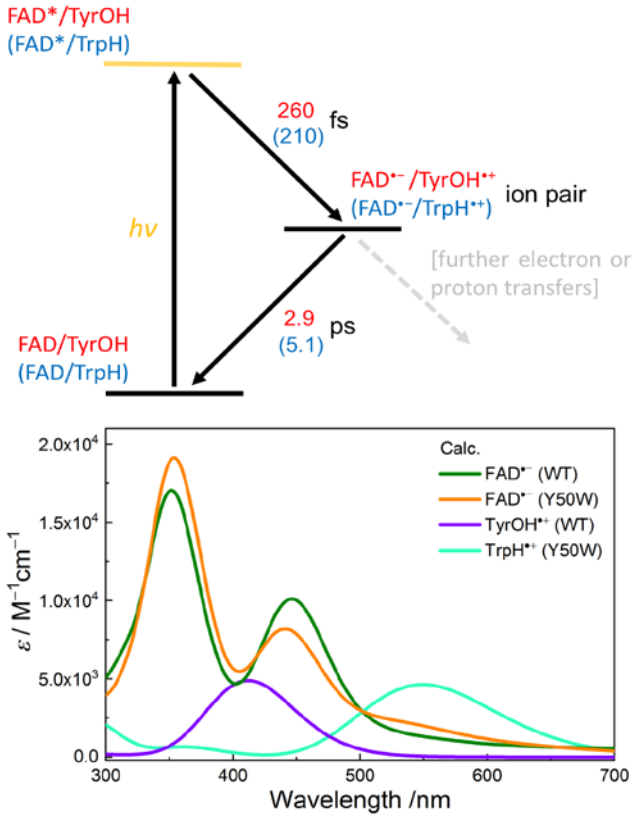

Figure 9. Calculated absorption spectra of individual radical intermediates involved in the light-induced processes of WT *Bs*FNR and the Y50W mutant.

QM/MM Spectral Simulations. The reaction scheme of the light-induced processes of WT and Y50W *Bs*FNR is summarized in Scheme 1. As indicated above, the products of the initial ET step can be unambiguously identified as charged radical pairs. However, the spectral properties have altered line shapes with respect to the reference spectra from other proteins or from solution. Moreover, even between WT and Y50W *Bs*FNR, $FAD^{\bullet-}$ appears to have different spectral features (Figure 6, absorption bands at ~ 400 and 520 nm), although this observation is complicated by different contributions from the amino acid radicals. In order to provide an interpretation framework of their spectral properties and explore the major effects that may lead to the spectral changes, we employed a QM/MM protocol to calculate the absorption spectra of $FAD^{\bullet-}$, $TyrOH^{\bullet+}$ and $TrpH^{\bullet+}$ in WT and Y50W *Bs*FNR (Figure 9). Despite some overestimations of the transition energies and oscillator strengths, the calculated spectra of $TrpH^{\bullet+}$ and $FAD^{\bullet-}$ qualitatively agree well with our experimental observations, and also provide a prediction of the $TyrOH^{\bullet+}$ absorption band. The discrepancies between experimental spectral and calculations probably arise from the limitation of TDDFT when it is applied to open-shell systems,[57] which is also observable for the spectrum of $TrpH^{\bullet+}$ calculated in solution (Figure 7, 13). The above-mentioned apparent differences in $FAD^{\bullet-}$ absorption bands between WT and Y50W *Bs*FNR (namely the relative amplitudes of the two absorption maxima) appear reproduced in the simulations; in addition substantial extension of the $FAD^{\bullet-}$ absorption in the red tail is modeled for both variants; these issues are subject to further assessments (*vide infra*).

We used the simulated spectra shown in Figure 9 to calculate the absorption spectra of the radical product states and compare them in Figure 10 with those deduced from the experimental EAS phases (see Section 5 of Supporting Information for details). Taking into account the abovementioned general limitation of TDDFT, our simulations faithfully reproduce the shape of the spectral features of $FAD^{\bullet-}/TyrOH^{\bullet+}$ and $FAD^{\bullet-}/TrpH^{\bullet+}$ ion pairs, thus supporting our interpretations of the respective recombination phases in WT and Y50W *Bs*FNR.

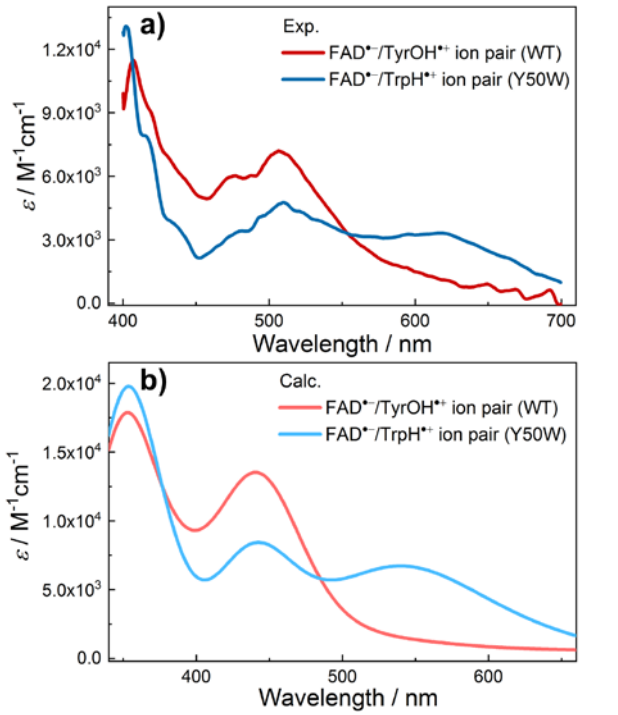

Figure 10. Experimentally determined absorption spectra (a) and calculated absorption spectra (b) of the $FAD^{\bullet-}/TyrOH^{\bullet+}$ and $FAD^{\bullet-}/TrpH^{\bullet+}$ ion pairs in *Bs*FNR. The experimental spectra during the light-induced processes of WT *Bs*FNR and the Y50W mutant were evaluated as described in Section 5 of Supporting Information. Simulated spectra of the ion pairs in WT *Bs*FNR and the Y50W mutant were computed by superimposing individual spectra of corresponding components shown in Figure 9. Wavelength range shown in panel (b) is different from panel (a) to account for a rigid shift (see text).

The substantial variation in $FAD^{\bullet-}$ spectra (Figure 7, 9) and shifts observed in the $TrpH^{\bullet+}$ spectrum with respect to the solution spectrum (Figure 8), imply that the local environment can have a significant impact on the spectral properties of the radical intermediates. In WT and Y50W *Bs*FNR, the active-site structures are presumably very much alike except for the presence of different counter-ions; the interactions between $FAD^{\bullet-}$

and $TyrOH^{\bullet+}$ or $TrpH^{\bullet+}$ thus should be of importance. As molecular absorption in the visible and near-infrared ranges are usually associated with electrons that occupy the frontier molecular orbitals (FMO), we calculated and visualized the HOMO(α), HOMO(β), LUMO(α) and LUMO(β) of $FAD^{\bullet-}$ in vacuum and in *Bs*FNR protein environments (Figure 11, S14). We note that among those FMO, in the protein environments the LUMO(α) of $FAD^{\bullet-}$, are significantly deformed compared with that in vacuum, which are mostly located beyond the molecular plane of FAD and extend toward the counter-ions. This result implies that electronic transitions of $FAD^{\bullet-}$ that involve this molecular orbital will exhibit strong charge-transfer characteristics. It also worth noting that they are shaped differently in WT *Bs*FNR and the Y50W mutant, which can reasonably explain the differences in $FAD^{\bullet-}$ spectra between these two variants. Contributions of MO pairs as well as hole-electron analysis of the lowest energy transition ($D_0 \rightarrow D_1$) of $FAD^{\bullet-}$ are described in Section 7 of Supporting Information (Figure S15), which provides a more detailed examination of the charge-transfer nature of this electronic transition.

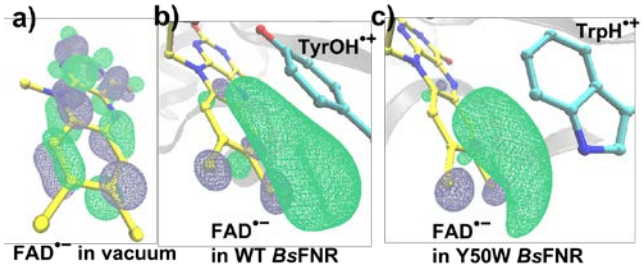

Figure 11. Calculated LUMO(α) (isovalue: 0.036) of $FAD^{\bullet-}$ in vacuum (a), in WT *Bs*FNR (b) and in the Y50W mutant (c) with the presence of corresponding counter-ions. The geometry of $FAD^{\bullet-}$ was energetically optimized at the QM level of theory (UB3LYP/6-311G*). Hydrogens are not shown for clarity.

To explicitly address the influence of the counter-ions, we calculated spectra of FAD, tyrosine and tryptophan in the radical anionic or cationic state with a unit probe point charge (e^+ for $FAD^{\bullet-}$, e^- for $TyrOH^{\bullet+}$ and $TrpH^{\bullet+}$) placed near the aromatic rings. The implicit solvent model with a dielectric constant ε=20 was used to simulate the screening effect of the protein/solvent environment. This approach strongly reduces the complexity of the systems but is representative enough to simulate the presence of counter-ions in a well-defined environment. As illustrated in Figure 12, the absorption spectra of $FAD^{\bullet-}$ are highly sensitive to the presence of the external positive point charge: when the distance between $FAD^{\bullet-}$ and the point charge reaches 5 Å, the absorption bands of $FAD^{\bullet-}$ start to change; with the decrease of the distance, the low-energy band increases its amplitude and red-shifts, while the high-energy band originally goes through a more complicated deformation, exhibiting an overall decrease of amplitude. These effects are in agreement with the main results of the spectral calculations in the complex explicit protein/solvent environment shown in Figure 9. They are approximately as expected from the spectral differences of $FAD^{\bullet-}$ between WT and Y50W *Bs*FNR, as in WT *Bs*FNR Tyr50 is located closer to FAD than Trp50 in the Y50W mutant.

On the other hand, noticeable changes in the calculated $TyrOH^{\bullet+}$ and $TrpH^{\bullet+}$ absorption spectra are only obtained when the negative point charge is placed as close as 2 Å. The contrasting behavior in $FAD^{\bullet-}$ *versus* $TyrOH^{\bullet+}$ and $TrpH^{\bullet+}$ could have two causes. First, a positive charge is likely to act as a virtual nucleus to attract electrons, strengthening the charge-transfer characteristics of the electronic transitions, and consequently leading to spectral deformations. This interpretation is supported by spectral calculations of $FAD^{\bullet-}$ with a negative point charge nearby, as well as $TyrOH^{\bullet+}$ and $TrpH^{\bullet+}$ with a positive charge nearby (Figure S16). Compared with the positive point charge, the negative point charge has limited effects on the spectrum of $FAD^{\bullet-}$; meanwhile, the spectrum of $TrpH^{\bullet+}$ starts to deform when the positive point charge is placed 3 Å away. Second, flavin has a larger and more complex π-conjugated system than tyrosine and tryptophan; in the radical anionic state, the unpaired electron tends to occupy molecular orbitals with higher energy than the unpaired electron in radical cationic molecules, and thus more inclined to be affected by the surrounding environment. Indeed, our DFT calculations confirm that $FAD^{\bullet-}$ has a much higher HOMO(α) (which corresponds to singly unoccupied molecular orbitals) energy than $TyrOH^{\bullet+}$ and $TrpH^{\bullet+}$ (–5.59, –12.49 and –11.21 eV in vacuum for $FAD^{\bullet-}$, $TyrOH^{\bullet+}$ and $TrpH^{\bullet+}$ respectively); the trend is also in agreement with the observation that the spectrum of $TyrOH^{\bullet+}$ is even more "inert" to the approach of the external charge than that of $TrpH^{\bullet+}$.

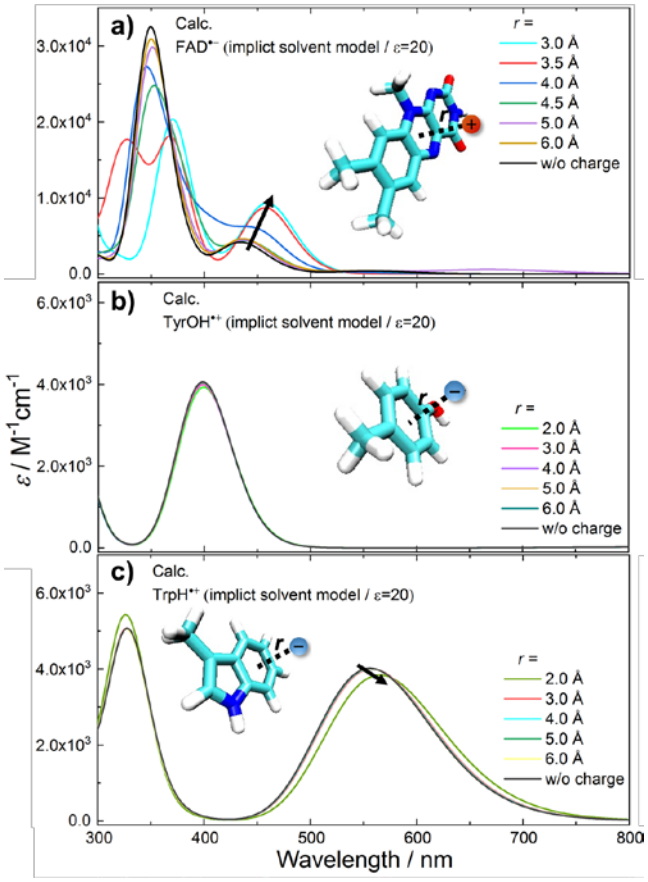

Figure 12. Distance-dependent effects of a unit point charge on the absorption spectra of $FAD^{\bullet-}$ (a), $TyrOH^{\bullet+}$ (b) and $TrpH^{\bullet+}$ (c). Structures of model compounds and the position of the probe charge (red: e^+, blue: e^-; above the geometric ring centers) are indicated in the insets.

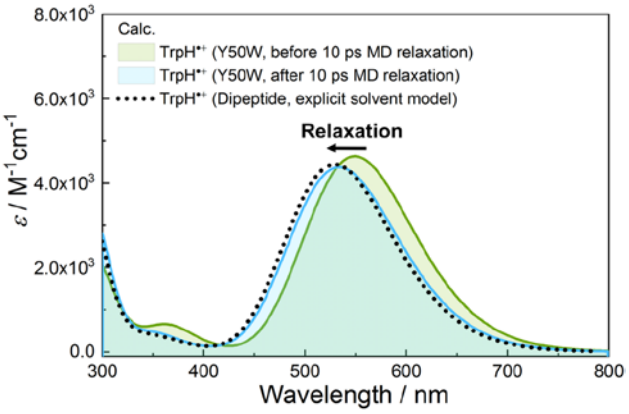

Figure 13. Calculated spectral charges of $TrpH^{\bullet+}$ following the relaxation process after the initial ET (averaged over 50 snapshots). As a reference the calculated $TrpH^{\bullet+}$ absorption spectrum in solution (explicit solvent model, structures of dipeptide for spectral calculations were taken from MD simulations with radical cationic geometry; the calculated spectrum corresponds to the average over 100 snapshots) is shown as the dotted line.

The effect of neighboring charges is expected to be much stronger and extending to larger distances in a hydrophobic environment, where no screening occurs (Figure S18). The spectrum calculated for $TrpH^{\bullet+}$ in Y50W *Bs*FNR (Figure 9) at first glance appears similar to that of $TrpH^{\bullet+}$ in solution (Figure 12). This could arise from the fact that in Y50W *Bs*FNR, Trp50 is located on the surface of the protein and exposed to the solvent. As demonstrated above charged species nearby have a moderate influence on the spectrum of $TrpH^{\bullet+}$ in a solvent-exposed protein environment. In Y50W *Bs*FNR the ring-to-ring distance is always larger than 3 Å (Figure 3), the influence of $FAD^{\bullet-}$ and surrounding residues on the absorption spectrum of $TrpH^{\bullet+}$ should be rather small. This suggestion seems to be at odds with the comparison of the transient experimental spectrum with the quasi-continuous reference spectrum of $TrpH^{\bullet+}$ in aqueous solution, obtained by pulse radiolysis, that are substantially shifted. We note that in our transient absorption measurement $TrpH^{\bullet+}$ decays in a few picoseconds upon formation, whereas the literature reference corresponds to equilibrated configurations. Experimentally, flavin spectral relaxations following photoexcitation on the picosecond timescale have been reported.[19,58] We therefore investigated whether configurational relaxations in the protein active site may influence the spectral properties of $TrpH^{\bullet+}$. To this end, we performed 10 ps MD simulations in the charge-separated state of Y50W *Bs*FNR starting from a neutral state molecular geometry. TDDFT calculations were carried out for $TrpH^{\bullet+}$ with the structures before and after the structural relaxation. Figure 13 clearly demonstrates that in Y50W *Bs*FNR, after the relaxation, the $D_0 \rightarrow D_2$ transition band of $TrpH^{\bullet+}$ shifts to shorter wavelengths, accompanied by a slight decrease in amplitude. Hence, during relaxation the positive charge of $TrpH^{\bullet+}$ induces polarization in the surrounding protein/solvent environment that stabilizes its positive charge. This induced polarization also destabilizes the LUMO, where the electron is closer to the negative charge induced in the environment, relative to the HOMO, and thus shifts the $D_0 \rightarrow D_2$ transition band to shorter wavelengths. Furthermore, as expected, the spectrum obtained after relaxation is similar to that calculated for the free radical ion in solution. These results qualitatively agree with our experimental observations. Within this interpretation, the apparent red-shift and line shape broadening of the $D_0 \rightarrow D_2$ transition band of $TrpH^{\bullet+}$ are most likely due to a combined effect of unrelaxed geometry (major) and the presence of the counter-ion $FAD^{\bullet-}$ (minor).

For completeness, similar relaxation effects were also calculated for the $TyrOH^{\bullet+}$ spectrum (Figure S19), although comparison with experimental relaxed spectra is not possible in this case.

DISCUSSION

We found that in WT *Bs*FNR the flavin excited state decays with a rate of ~4.0 ps^{-1} due to electron transfer to the close by tyrosine residue. This rate is similar to that in a number of other proteins where flavin fluorescence is quenched by nearby aromatic residues.[7–9,16,58] Yet, of these, studies with full spectral characterization of the products with tyrosine as a quencher are limited to recent studies on TrmFO.[26,27] The found rate of FAD photoreduction in WT *Bs*FNR is faster than that observed in TrmFO (*Tt*TrmFO: 0.9 ps^{-1}; *Bs*TrmFO: 2.7 ps^{-1}). The difference is likely due to a closer stacking of the tyrosine residue and FAD in *Bs*FNR than in *Tt*TrmFO (for which a structure is available), maintained by a H-bond interaction in addition to steric interactions with other surrounding residues, allowing a stronger electronic interaction between the donor and acceptor, *i.e.*, a larger electronic coupling term.[1,59]

In WT and Y50W *Bs*FNR, the charge-separated product states both decay mainly by charge recombination in a few picoseconds (WT: 0.3 ps^{-1}; Y50W: 0.2 ps^{-1}), similarly as in other flavoproteins with nearby aromatic residues.[10,23,27,28] Qualitatively, the somewhat higher rate of the back ET in WT *Bs*FNR may be related to the shorter average donor-acceptor distance (Figure 3), and the larger driving force due to the higher redox potential of tyrosine in proteins.[7]

The significant separation of timescales of the dominant excited state decay and product decay allowed to unambiguously determine the transient spectrum of the initial photoproduct of WT *Bs*FNR. It is similar to that reported for TrmFO,[26,27] with $TyrOH^{\bullet+}$ absorption strongly contributing to the observed EAS of the product state, confirming that in a confined protein environment without suitable proton acceptors and on an ultrafast timescale, despite its extremely high acidity, $TyrOH^{\bullet+}$ can be formed as a distinct species without concomitant deprotonation.

In WT *Bs*FNR the contributions of both constituents of the $FAD^{\bullet-}$/$TyrOH^{\bullet+}$ product states appear to overlap. For the Y50W mutant, the $TrpH^{\bullet+}$ product absorbs more to longer wavelengths and was further analyzed by comparing experimental and simulation results. Here, the $TrpH^{\bullet+}$ spectrum was found to extend more to longer wavelengths than the model spectrum obtained on the microsecond timescale in aqueous solution that is extensively used in the literature. Nevertheless, our simulations based on relaxed geometries suggest that, with Trp50 being exposed to the solvent in Y50W *Bs*FNR, the $TrpH^{\bullet+}$ spectrum should be quasi-indistinguishable from the solution spectrum. Our further simulations suggest that this discrepancy is related to the fact that the structure is not fully relaxed on the timescale of the lifetime of the charge-separated state of a few picoseconds. This assessment is in general agreement with experimental evidence that charge relaxations influencing electronic spectra occur on

this timescale, including in flavoproteins,[19,58] and as also observed in the excited state of the Y50G *Bs*FNR construct (Figure S7c). Vibrational relaxation has also been invoked to qualitatively explain blue-shifting of $TrpH^{\bullet+}$ spectra on the picosecond timescale in cryptochromes and photolyases.[23,60]

We note that in DNA photolyase from *Escherichia coli* the spectrum of the solvent-exposed $TrpH^{\bullet+}$ on the nanosecond timescale, generated from the resting $FADH^{\bullet}$ state can be well modelled with the solvent spectrum.[14] The corresponding spectra generated from the $FAD^{\bullet-}$ state in this enzyme[61] and in algal cryptochrome/photolyase enzymes[16,23] on the tens and hundreds of picoseconds timescale appear more red-extended. This may be due to inhomogeneities in the initially populated excited states, as demonstrated for the *Ostreococcus tauri* enzyme. In view of the demonstrated sensitivity of the $FAD^{\bullet-}$ spectrum to the surrounding environment (Figure 12a), as well as the strongly red-extending tail in our calculated spectrum (Figure 9) that most likely results from charge-transfer excitations (Figure S15), it also appears conceivable that contributions of the $FAD^{\bullet-}$ spectrum play a role. Moreover, as the spectral properties of $FAD^{\bullet-}$ are highly sensitive to protein environments, applying model spectra of $FAD^{\bullet-}$ from different flavoproteins (or even different variants of the same protein) for spectral analysis should be handled with caution.

Finally, the experiments on the Y50G mutant shed light on the effect of product ($NADP^+$) binding to the active site of *Bs*FNR. In the absence of the $NADP^+$ product, the FAD^* decay is bi-exponential, with a significant fraction having a time constant of ~300 ps, which is an order of magnitude faster than the intrinsic flavin fluorescence decay observed for the other main fraction. The faster phase presumably corresponds to a configuration where electron transfer from further lying (than Tyr50) aromatic amino acids can occur. In the presence of the product, this faster phase is not observed, and mono-exponential decay occurs. This finding thus suggests that product binding abolishes structural heterogeneity and leads to a less flexible active site. A more flexible active site in the absence of reactant may help binding of the aromatic substrate molecules; and its arrest in a specific configuration in the presence of product (and presumably substrate) may favor the enzymatic reaction, as discussed for instance for the flavoprotein ThyX.[19]

Altogether, using a combination of ultrafast spectroscopies and simulation methods to study the photoproducts of *Bs*FNR has allowed us to get insight in the spectral properties of radical intermediates that deviate from model spectra. Our results may help to understand similar features in a range of flavoprotein systems.

ASSOCIATED CONTENT

Supporting Information

The Supporting Information is available free of charge on the ACS Publications website.

Spectral and structural properties of *Bs*FNR in the ground-state; effects of $NADP^+$ binding on the fluorescence decay; full EAS from global fitting of transient absorption data; determination of the initial concentrations of FAD^* in transient absorption measurements; extraction of the absorption spectra of ion pairs; system preparation for spectral calculations; additional results of spectral calculations.

AUTHOR INFORMATION

Corresponding Authors

* alexey.aleksandrov@polytechnique.edu (A. A.)

* marten.vos@polytechnique.edu (M. H. V.)

Notes

The authors declare no competing financial interest.

ACKNOWLEDGMENTS

This work was partly supported by Japan Society for the Promotion of Science KAKENHI Grant Number JP17K07304 (to D. S.). B. Z. thanks the China Scholarship Council for providing a PhD scholarship.

REFERENCES

(1) Gray, H. B.; Winkler, J. R. Electron Tunneling through Proteins. Q. Rev. Biophys. **2003**, *36* (3), 341–372.

(2) Lukacs, A.; Eker, A. P. M.; Byrdin, M.; Brettel, K.; Vos, M. H. Electron Hopping through the 15 Å Triple Tryptophan Molecular Wire in DNA Photolyase Occurs within 30 ps. *J. Am. Chem. Soc.* **2008**, *130* (44), 14394–14395.

(3) Minnihan, E. C.; Nocera, D. G.; Stubbe, J. A. Reversible, Long-Range Radical Transfer in E. Coli Class Ia Ribonucleotide Reductase. *Acc. Chem. Res.* **2013**, *46* (11), 2524–2535.

(4) Geng, J.; Dornevil, K.; Davidson, V. L.; Liu, A. Tryptophan-Mediated Charge-Resonance Stabilization in the Bis-Fe(IV) Redox State of MauG. *Proc. Natl. Acad. Sci. U. S. A.* **2013**, *110* (24), 9639–9644.

(5) Dempsey, J. L.; Winkler, J. R.; Gray, H. B. Proton-Coupled Electron Flow in Protein Redox Machines. *Chem. Rev.* **2010**, *110* (12), 7024–7039.

(6) Tian, S.; Jones, S. M.; Solomon, E. I. Role of a Tyrosine Radical in Human Ceruloplasmin Catalysis. *ACS Cent. Sci.* **2020**, *6* (10), 1835–1843

(7) Mataga, N.; Chosrowjan, H.; Shibata, Y.; Tanaka, F.; Nishina, Y.; Shiga, K. Dynamics and Mechanisms of Ultrafast Fluorescence Quenching Reactions of Flavin Chromophores in Protein Nanospace. *J. Phys. Chem. B* **2000**, *104* (45), 10667–10677.

(8) Nunthaboot, N.; Tanaka, F.; Kokpol, S.; Chosrowjan, H.; Taniguchi, S.; Mataga, N. Simultaneous Analysis of Ultrafast Fluorescence Decays of FMN Binding Protein and Its Mutated Proteins by Molecular Dynamic Simulation and Electron Transfer Theory. *J. Phys. Chem. B* **2008**, *112* (41), 13121–13127.

(9) Mataga, N.; Chosrowjan, H.; Taniguchi, S.; Tanaka, F.; Kido, N.; Kitamura, M. Femtosecond Fluorescence Dynamics of Flavoproteins: Comparative Studies on Flavodoxin, Its Site-Directed Mutants, and Riboflavin Binding Protein Regarding Ultrafast Electron Transfer in Protein Nanospaces. *J. Phys. Chem. B* **2002**, *106* (35), 8917–8920.

(10) Zhong, D.; Zewail, A. H. Femtosecond Dynamics of Flavoproteins: Charge Separation and Recombination in Rioboflavin (Vitamin B2)-Binding Protein and in Glucose Oxidase Enzyme. *Proc. Natl. Acad. Sci. U.S.A.* **2001**, *98* (21), 11867–11872.

(11) Pan, J.; Byrdin, M.; Aubert, C.; Eker, A. P. M.; Brettel, K.; Vos, M. H. Excited-State Properties of Flavin Radicals in Flavoproteins: Femtosecond Spectroscopy of DNA Photolyase, Glucose Oxidase, and Flavodoxin. **2004**, *108* (28), 10160–10167

(12) Kundu, M.; He, T. F.; Lu, Y.; Wang, L.; Zhong, D. Short-Range Electron Transfer in Reduced Flavodoxin: Ultrafast Nonequilibrium Dynamics Coupled with Protein Fluctuations. *J. Phys. Chem. Lett.* **2018**, *9* (11), 2782–2790.

(13) Zanetti-Polzi, L.; Aschi, M.; Amadei, A.; Daidone, I. Alternative Electron-Transfer Channels Ensure Ultrafast Deactivation of Light-

Induced Excited States in Riboflavin Binding Protein. *J. Phys. Chem. Lett.* **2017**, *8*

(14), 3321–3327.(14) Aubert, C.; Vos, M. H.; Mathis, P.; Eker, A. P. M.; Brettel, K. Intra-Protein Radical Transfer during Photoactivation of DNA Photolyase. *Nature* **2000**, *405*, 586–590.

(15) Brettel, K.; Byrdin, M.; Vos, M. H. Ultrafast Light-Induced Processes in DNA-Photolyase and Its Substrate-Bound Complex. In Ultrafast Dynamics at the Nanoscale: Biomolecules and Supramolecular Assemblies; Haacke, S., Burghardt, I., Eds.; Pan Stanford: Singapore, **2016**; pp 65–90.

(16) Brazard, J.; Usman, A.; Lacombat, F.; Ley, C.; Martin, M. M.; Plaza, P.; Mony, L.; Heijde, M.; Zabulon, G.; Bowler, C. Spectro-Temporal Characterization of the Photoactivation Mechanism of Two New Oxidized Cryptochrome/Photolyase Photoreceptors. *J. Am. Chem. Soc.* **2010**, *132* (13), 4935–4945.

(17) Lukacs, A.; Brust, R.; Haigney, A.; Laptenok, S. P.; Addison, K.; Gil, A.; Towrie, M.; Greetham, G. M.; Tonge, P. J.; Meech, S. R. BLUF Domain Function Does Not Require a Metastable Radical Intermediate State. *J. Am. Chem. Soc.* **2014**, *136* (12), 4605–4615.

(18) Gauden, M.; Grinstead, J. S.; Laan, W.; van Stokkum, I. H. M.; Avila-Perez, M.; Toh, K. C.; Boelens, R.; Kaptein, R.; van Grondelle, R.; Hellingwerf, K. J.; Kennis, J. T. M. On the Role of Aromatic Side Chains in the Photoactivation of BLUF Domains. *Biochemistry* **2007**, *46* (25), 7405–7415.

(19) Laptenok, S. P.; Bouzhir-Sima, L.; Lambry, J.-C.; Myllykallio, H.; Liebl, U.; Vos, M. H. Ultrafast Real Time Visualization of the Active Site Flexibility of the Flavoenzyme Thymidylate Synthase ThyX. *Proc. Natl. Acad. Sci. U.S.A.* **2013**, *110*, 8924–8929.

(20) Yang, H.; Luo, G.; Karnchanaphanurach, P.; Louie, T.-M.; Rech, I.; Cova, S.; Xun, L.; Xie, X. S. Protein Conformational Dynamics Probed by Single-Molecule Electron Transfer. *Science* **2003**, *302* (5643), 262–266.

(21) Aubert, C.; Mathis, P.; Eker, A. P. M.; Brettel, K. Intraprotein Electron Transfer between Tyrosine and Tryptophan in DNA Photolyase from Anacystis Nidulans. *Proc. Natl. Acad. Sci. U.S.A.* **1999**, *96* (10), 5423–5427.

(22) Immeln, D.; Weigel, A.; Kottke, T.; Pérez Lustres, J. L. Primary Events in the Blue Light Sensor Plant Cryptochrome: Intraprotein Electron and Proton Transfer Revealed by Femtosecond Spectroscopy. *J. Am. Chem. Soc.* **2012**, *134* (30), 12536–12546.

(23) Lacombat, F.; Espagne, A.; Dozova, N.; Plaza, P.; Müller, P.; Brettel, K.; Franz-Badur, S.; Essen, L. O. Ultrafast Oxidation of a Tyrosine by Proton-Coupled Electron Transfer Promotes Light Activation of an Animal-like Cryptochrome. *J. Am. Chem. Soc.* **2019**, *141* (34), 13394–13409.

(24) Bialas, C.; Jarocha, L. E.; Henbest, K. B.; Zollitsch, T. M.; Kodali, G.; Timmel, C. R.; Mackenzie, S. R.; Dutton, P. L.; Moser, C. C.; Hore, P. J. Engineering an Artificial Flavoprotein Magnetosensor. *J. Am. Chem. Soc.* **2016**, *138* (51), 16584–16587.

(25) Bialas, C.; Barnard, D. T.; Auman, D. B.; Mcbride, R. A.; Jarocha, L. E.; Hore, P. J.; Dutton, P. L.; Stanley, R. J.; Moser, C. C. Ultrafast Flavin/Tryptophan Radical Pair Kinetics in a Magnetically Sensitive Artificial Protein. *Phys. Chem. Chem. Phys.* **2019**, *21*, 13453–13461.

(26) Dozova, N.; Lacombat, F.; Bou-Nader, C.; Hamdane, D.; Plaza, P. Ultrafast Photoinduced Flavin Dynamics in the Unusual Active Site of the tRNA Methyltransferase TrmFO. *Phys. Chem. Chem. Phys.* **2019**, *21*, 8743–8756.

(27) Nag, L.; Sournia, P.; Myllykallio, H.; Liebl, U.; Vos, M. H. Identification of the TyrOH•+ Radical Cation in the Flavoenzyme TrmFO. *J. Am. Chem. Soc.* **2017**, *139* (33), 11500–11505.

(28) Nag, L.; Lukacs, A.; Vos, M. H. Short-Lived Radical Intermediates in the Photochemistry of Glucose Oxidase. *ChemPhysChem* **2019**, *20* (14), 1793–1798.

(29) Seo, D.; Kamino, K.; Inoue, K.; Sakurai, H. Purification and Characterization of Ferredoxin-NADP+ Reductase Encoded by Bacillus Subtilis yumC. *Arch. Microbiol.* **2004**, *182* (1), 80–89.

(30) Seo, D.; Asano, T.; Komori, H.; Sakurai, T. Role of the C-Terminal Extension Stacked on the Re-Face of the Isoalloxazine Ring Moiety of the Flavin Adenine Dinucleotide Prosthetic Group in Ferredoxin-NADP+ Oxidoreductase from Bacillus Subtilis. *Plant Physiol. Biochem.* **2014**, *81*, 143–148.

(31) Seo, D.; Soeta, T.; Sakurai, H.; Sétif, P.; Sakurai, T. Pre-Steady-State Kinetic Studies of Redox Reactions Catalysed by Bacillus Subtilis Ferredoxin-NADP+ Oxidoreductase with NADP+/NADPH and Ferredoxin. *Biochim. Biophys. Acta* **2016**, *1857* (6), 678–687.

(32) Komori, H.; Seo, D.; Sakurai, T.; Higuchi, Y. Crystal Structure Analysis of Bacillus Subtilis Ferredoxin-NADP+ Oxidoreductase and the Structural Basis for Its Substrate Selectivity. *Protein Sci.* **2010**, *19* (12), 2279–2290.

(33) Seo, D.; Naito, H.; Nishimura, E.; Sakurai, T. Replacement of Tyr50 Stacked on the Si-Face of the Isoalloxazine Ring of the Flavin Adenine Dinucleotide Prosthetic Group Modulates Bacillus Subtilis Ferredoxin-NADP+ Oxidoreductase Activity toward NADPH. *Photosynth. Res.* **2015**, *125* (1), 321–328.

(34) Cailliez, F.; Müller, P.; Firmino, T.; Pernot, P.; De La Lande, A. Energetics of Photoinduced Charge Migration within the Tryptophan Tetrad of an Animal (6-4) Photolyase. *J. Am. Chem. Soc.* **2016**, *138* (6), 1904–1915.

(35) Laptenok, S. P.; Nuernberger, P.; Lukacs, A.; Vos, M. H.; Walker, J. M. Subpicosecond Kerr-Gate Spectrofluorometry. In Methods in Molecular Biology, Fluorescence Spectroscopy and Microscopy: Methods and Protocols, Vol. 1076; Engelborghs, Y., Visser, A. J. W. G., Eds.; Humana Press: New York, **2014**; pp 321–336.

(36) Byrdin, M.; Lukacs, A.; Thiagarajan, V.; Eker, A. P. M.; Brettel, K.; Vos, M. H. Quantum Yield Measurements of Short-Lived Photoactivation Intermediates in DNA Photolyase: Toward a Detailed Understanding of the Triple Tryptophan Electron Transfer Chain. *J. Phys. Chem. A* **2010**, *114* (9), 3207–3214.

(37) Snellenburg, J. J.; Laptenok, S. P.; Seger, R.; Mullen, K. M.; van Stokkum, I. H. M. Glotaran: A Java-Based Graphical User Interface for the R Package TIMP. *J. Stat. Softw.* **2012**, 49 (3).

(38) Phillips, J. C.; Braun, R.; Wang, W.; Gumbart, J.; Tajkhorshid, E.; Villa, E.; Chipot, C.; Skeel, R. D.; Kalé, L.; Schulten, K. Scalable Molecular Dynamics with NAMD. *J. Comput. Chem.* **2005**, *26* (16), 1781–1802.

(39) Huang, J.; Mackerell, A. D. CHARMM36 All-Atom Additive Protein Force Field: Validation Based on Comparison to NMR Data. *J. Comput. Chem.* **2013**, *34* (25), 2135–2145.

(40) Jorgensen, W. L.; Chandrasekhar, J.; Madura, J. D.; Impey, R. W.; Klein, M. L. Comparison of Simple Potential Functions for Simulating Liquid Water. *J. Chem. Phys.* **1983**, *79* (2), 926–935.

(41) Aleksandrov, A. A Molecular Mechanics Model for Flavins. *J. Comp. Chem.* **2019**, *40* (32), 2834–2842.

(42) Krivov, G. G.; Shapovalov, M. V.; Dunbrack, R. L. Improved Prediction of Protein Side-Chain Conformations with SCWRL4. *Proteins Struct. Funct. Bioinforma.* **2009**, 77 (4), 778–795.

(43) Breneman, C. M.; Wiberg, K. B. Determining Atom-centered Monopoles from Molecular Electrostatic Potentials. The Need for High Sampling Density in Formamide Conformational Analysis. *J. Comput. Chem.* **1990**, *11* (3), 361–373.

(44) Field, M. J. The PDynamo Program for Molecular Simulations Using Hybrid Quantum Chemical and Molecular Mechanical Potentials. *J. Chem. Theory Comput.* **2008**, *4* (7), 1151–1161.

(45) Neese, F. The ORCA Program System. *Wiley Interdiscip. Rev. Comput. Mol. Sci.* **2012**, *2* (1), 73–78.

(46) Becke, A. D. A New Mixing of Hartree-Fock and Local Density-Functional Theories. *J. Chem. Phys.* **1993**, *98* (2), 1372–1377.

(47) Krishnan, R.; Binkley, J. S.; Seeger, R.; Pople, J. A. Self-Consistent Molecular Orbital Methods. XX. A Basis Set for Correlated Wave Functions. *J. Chem. Phys.* **1980**, *72* (1), 650–654.

(48) Barone, V.; Cossi, M. Quantum Calculation of Molecular Energies and Energy Gradients in Solution by a Conductor Solvent Model. *J. Phys. Chem. A* **1998**, *102* (11), 1995–2001.

(49) Lostao, A.; Gómez-Moreno, C.; Mayhew, S. G.; Sancho, J. Differential Stabilization of the Three FMN Redox Forms by Tyrosine 94 and Tryptophan 57 in Flavodoxin from Anabaena and Its Influence on the Redox Potentials. *Biochemistry* **1997**, *36* (47), 14334–14344.

(50) Medina, M., and Gómez-Moreno, C. Interaction of ferredoxin-NADP+ reductase with its substrates: optimal interaction for efficient electron transfer, *Photosynth. Res.* **2004**, *79*, 113-131.

(51) Aliverti, A., Pandini, V., Pennati, A., de Rosa, M., and Zanetti, G. Structural and functional diversity of ferredoxin-NADP(+) reductases. *Arch. Biochem. Biophys.* **2008**, *474* (2), 283−291.

(52) York, N.; Massey, V.; Palmer, G. On the Existence of Spectrally Distinct Classes of Flavoprotein: A New Method for the Quantitative Production of Flavoprotein Semiquinones. *Biochemistry* **1966**, *5* (10), 3181–3189

(53) Liu, B.; Liu, H.; Zhong, D.; Lin, C. Searching for a Photocycle of the Cryptochrome Photoreceptors. *Curr. Opin. Plant Biol.* **2010**, *13* (5), 578–586.

(54) Gräslund, A.; Sahlin, M.; Sjöberg, B.-M. The Tyrosyl Free Radical in Ribonucleotide Reductase. *Env. Heal. Persp.* **1985**, *64*, 139–149.

(55) Müller, P.; Bouly, J.-P.; Hitomi, K.; Balland, V.; Getzoff, E. D.; Ritz, T.; Brettel, K. ATP Binding Turns Plant Cryptochrome Into an Efficient Natural Photoswitch. *Sci. Rep.* **2014**, *4*, 5175.

(56) Solar, S.; Getoff, N.; Surdhar, P. S.; Armstrong, D. A.; Singh, A. Oxidation of Tryptophan and N-Methylindole by N3●, Br2●-, and (SCN)2●- Radicals in Light- and Heavy-Water Solutions: A Pulse Radiolysis Study. *J. Phys. Chem.* **1991**, *95* (9), 3639–3643.

(57) Rgen Fabian, J. TDDFT-Calculations of Vis/NIR Absorbing Compounds. *Dyes Pigm.* **2010**, *84* (1), 36–53

(58) He, T. F.; Guo, L.; Guo, X.; Chang, C. W.; Wang, L.; Zhong, D. Femtosecond Dynamics of Short-Range Protein Electron Transfer in Flavodoxin. *Biochemistry* **2013**, *52* (51), 9120–9128.

(59) Liu, J.; Chakraborty, S.; Hosseinzadeh, P.; Yu, Y.; Tian, S.; Petrik, I.; Bhagi, A.; Lu, Y. Metalloproteins Containing Cytochrome, Iron–Sulfur, or Copper Redox Centers. *Chem. Rev.* **2014**, *114*, 4366–4469.

(60) Martin, R.; Lacombat, F.; Espagne, A.; Dozova, N.; Plaza, P.; Yamamoto, J.; Müller, P.; Brettel, K.; De La Lande, A. Ultrafast Flavin Photoreduction in an Oxidized Animal (6-4) Photolyase through an Unconventional Tryptophan Tetrad. *Phys. Chem. Chem. Phys.* **2017**, *19* (36), 24493–24504.

(61) Liu, Z.; Tan, C.; Guo, X.; Li, J.; Wang, L.; Sancar, A.; Zhong, D. Determining Complete Electron Flow in the Cofactor Photoreduction of Oxidized Photolyase. *Proc. Natl. Acad. Sci. U. S. A.* **2013**, *110* (32), 12966–12971.

For Table of Contents Only